LETTER

doi:10.1038/nature13734

Probing excitonic dark states in single-layer tungsten disulphide

Ziliang Ye[1]*, Ting Cao[2,3]*, Kevin O'Brien[1], Hanyu Zhu[1], Xiaobo Yin[1], Yuan Wang[1], Steven G. Louie[2,3] & Xiang Zhang[1,3,4,5]

Transition metal dichalcogenide (TMDC) monolayers have recently emerged as an important class of two-dimensional semiconductors with potential for electronic and optoelectronic devices[1,2]. Unlike semimetallic graphene, layered TMDCs have a sizeable bandgap[3]. More interestingly, when thinned down to a monolayer, TMDCs transform from indirect-bandgap to direct-bandgap semiconductors[4,5], exhibiting a number of intriguing optical phenomena such as valley-selective circular dichroism[6–8], doping-dependent charged excitons[9,10] and strong photocurrent responses[11]. However, the fundamental mechanism underlying such a strong light–matter interaction is still under intensive investigation. First-principles calculations have predicted a quasiparticle bandgap much larger than the measured optical gap, and an optical response dominated by excitonic effects[12–14]. In particular, a recent study based on a GW plus Bethe–Salpeter equation (GW-BSE) approach, which employed many-body Green's-function methodology to address electron–electron and electron–hole interactions, theoretically predicted a diversity of strongly bound excitons[14]. Here we report experimental evidence of a series of excitonic dark states in single-layer WS_2 using two-photon excitation spectroscopy. In combination with GW-BSE theory, we prove that the excitons are of Wannier type, meaning that each exciton wavefunction extends over multiple unit cells, but with extraordinarily large binding energy (~0.7 electronvolts), leading to a quasiparticle bandgap of 2.7 electronvolts. These strongly bound exciton states are observed to be stable even at room temperature. We reveal an exciton series that deviates substantially from hydrogen models, with a novel energy dependence on the orbital angular momentum. These excitonic energy levels are experimentally found to be robust against environmental perturbations. The discovery of excitonic dark states and exceptionally large binding energy not only sheds light on the importance of many-electron effects in this two-dimensional gapped system, but also holds potential for the device application of TMDC monolayers and their heterostructures[15] in computing, communication and bio-sensing.

An exciton is a bound state formed by an excited electron and hole owing to the Coulomb attraction between these two quasiparticles[16]. Such bound states often play an important role in the optical properties of low-dimensional materials[17], owing to their strong spatial confinement and reduced screening effect compared to bulk solids. In a two-dimensional (2D) gapped system with dipole-allowed interband transitions, the optical absorption spectrum in the non-interacting limit exhibits a step function. Strong electron–hole interaction redshifts a large amount of the spectral weight, resulting in a qualitatively different spectrum with a series of new excitonic levels below the quasiparticle bandgap. In quasi-2D quantum wells, the electron–hole interaction is weak. Therefore, by measuring the energy difference between the first excitonic peak and band-edge absorption step, the exciton binding energy can be unambiguously determined; it usually has an energy of tens of meV and is vulnerable to environment screening and temperature broadening. However, recent experiments on a single-layer TMDC like MoS_2 found no absorption step[4,5]. Instead, two absorption peaks from spin–orbit splitting were detected[4,5] around the Kohn–Sham bandgap energy, as given by density functional theory (DFT) within the local density approximation. The peaks were initially interpreted as direct band edge transitions. In sharp contrast, more accurate first-principles calculations on MoS_2 monolayer using the GW method[18] predicted a quasiparticle bandgap that was larger than the initial experimental reported value by nearly one electronvolt[12–14]. Relevant calculations based on first-principles GW-BSE theory[19] showed this energy gap discrepancy to originate in strong excitonic effects. It is therefore critical to uncover the underlying physics of the strong light–matter interaction in such a 2D system.

We probed the excitonic effects in monolayer WS_2, also an important TMDC material, using two-photon excitation spectroscopy[20]. At the simplest level, if an electron–hole pair interacts through a Coulomb attractive central potential, it will form a series of excitonic Rydberg-like states with definite parity, similar to the hydrogen model. For WS_2, the breaking of rotational and inversion symmetry owing to the crystal structure and the spatial dependence of screening will modify the energy and symmetry of the states from those of the 2D Rydberg series. However, for exciton states with an electron–hole wavefunction that is large compared to the unit cell size (as shown below for WS_2), specific parity may still be assigned to each excitonic state. Incident photons can excite the electronic system from the ground state to one of these excitonic states (Fig. 1a). In addition to energy conservation, the selection rule of such a transition depends on the symmetry of the final state: for systems with dipole-allowed interband transitions (which is the case for WS_2), one-photon transitions can only reach excitonic states with even parity, while two-photon transitions reach states with odd parity. The two-photon resonances are also known as excitonic dark states as they do not appear in the linear optical spectrum. These dark states are good gauges for excitonic effects, since there is little impurity and bandgap absorption background in the two-photon spectrum. Owing to the direct bandgap in this WS_2 monolayer, we monitor the two-photon absorption induced luminescence (which we abbreviate to two-photon luminescence, TPL) with a high signal-to-noise ratio. The luminescence results from the radiative recombination of the excitonic ground state, following the rapid non-radiative relaxation from the two-photon excited excitonic dark states to the exciton ground state (Fig. 1a). By scanning the excitation laser energy, we obtain a complete two-photon spectrum, assuming the relaxation and emission efficiency are independent of the excitation energy.

Our samples are WS_2 monolayers directly exfoliated on fused quartz substrates. A typical light emission spectrum is shown in Fig. 1b, excited by an ultrafast laser (pulses of 190 fs duration) at a wavelength of 990 nm (1.25 eV) at a sample temperature of 10 K. The two peaks observed at 2.0 eV and 2.04 eV correspond to the exciton and negatively charged trion emissions from the direct bandgap at K and K′ valleys in the Brillouin zone, consistent with the absorption peaks in the reflectance spectrum (Supplementary Information section S1) The emitted photon energies of both peaks are much higher than those of the excitation photon, and

[1]NSF Nano-scale Science and Engineering Center (NSEC), 3112 Etcheverry Hall, University of California, Berkeley, California 94720, USA. [2]Department of Physics, University of California, Berkeley, California 94720, USA. [3]Material Sciences Division, Lawrence Berkeley National Laboratory, 1 Cyclotron Road, Berkeley, California 94720, USA. [4]Department of Physics, King Abdulaziz University, Jeddah 21589, Saudi Arabia. [5]Kavli Energy NanoSciences Institute at the University of California, Berkeley, and Lawrence Berkeley National Laboratory, Berkeley, California 94704, USA.
*These authors contributed equally to this work.

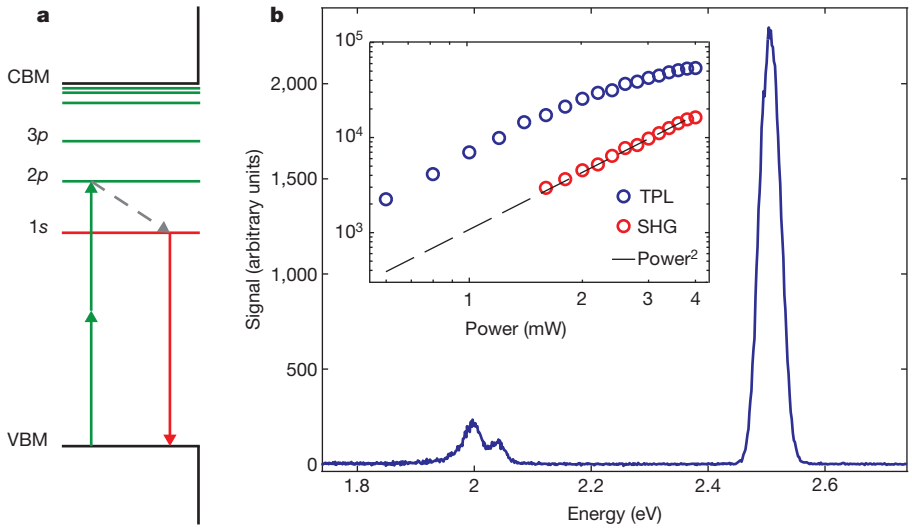

Figure 1 | Probing the dark exciton states in single-layer WS_2 by two-photon luminescence. **a**, Schematic of the two-photon luminescence (TPL) process in single-layer WS_2. Under two-photon excitation, electrons transition to one of the excitonic dark states with odd parity (double green arrow). Following the excitation, the exciton experiences a fast relaxation to the excitonic ground state (grey arrow) and emits a photon (red arrow). The two-photon selection rule exclusively eliminates the one-photon transition background and reveals the excitonic excited states. States are labelled *s* (red) or *p* (green) according to the excitonic envelope wavefunction character. CBM and VBM represent respectively the conduction band minimum and the valence band maximum. **b**, Main panel: measured WS_2 emission spectrum excited by an ultrafast pulsed laser at 10 K. The peaks at 2.04 eV and 2 eV are the A exciton (1*s* state) and its trion peak, respectively. The lower-energy peak is stronger than the higher-energy one due to the exciton–trion equilibrium reached during the emission stage at low temperature. The excitation pulse is at 1.25 eV with a pulse width of about 190 ± 20 fs, which results in the 2.5 eV peak as the SHG signal. Inset, the power dependence of the SHG and TPL signals. At a low excitation level, both of them exhibit quadratic power dependence, confirming the two-photon absorption nature of the luminescence, until the TPL signal saturates at a high excitation level. The TPL signal represents the amplitude of the trion peak.

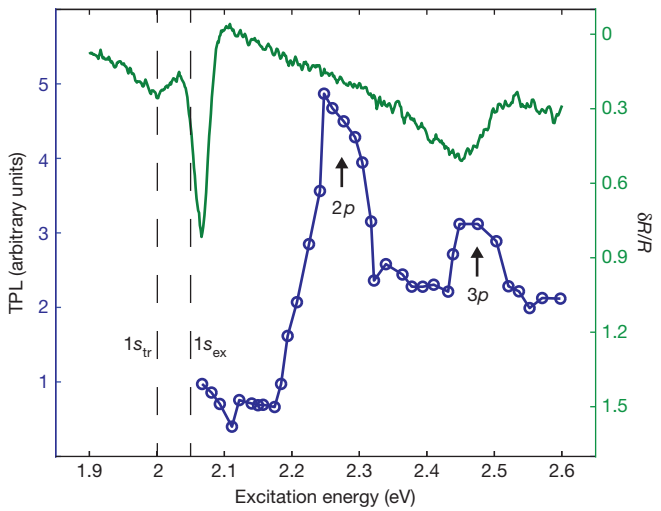

Figure 2 | Extraordinarily strong excitonic effect in monolayer WS_2. Two-photon absorption (blue) and one-photon absorption (green) spectra are measured in single-layer WS_2 at 10 K. In the two-photon absorption spectrum, 2*p* and 3*p* resonances are observed at 2.28 eV and 2.48 eV, respectively, on top of a plateau background. For comparison, the one-photon absorption spectrum, measured as the relative reflectance signal ($\delta R/R$), exhibits no corresponding features except a B exciton (1*s*) related absorption resonance at 2.45 eV. Additionally, the A exciton ($1s_{ex}$) and trion ($1s_{tr}$) absorption peaks are detected consistently with the TPL emission peaks (Fig. 1b), with a 20 meV Stoke shift, and are marked at 2.04 and 2 eV, respectively, by black dashed lines. The energy difference between the A exciton 1*s* state emission peak and the 3*p* state absorption peak is 0.44 eV, which yields the lower bound for the exciton binding energy in monolayer WS_2. This binding energy is extraordinarily large for a Wannier exciton, and implies a dominating excitonic mechanism for the intense light–matter interaction in 2D TMDCs. The total excitation scan is achieved by tuning an output beam of an optical parametric oscillator over a 600 meV span, with a scanning resolution of about 15 meV (Supplementary Information section S3). Similar results are repeated in more than 5 flakes.

therefore they can only originate from TPL. The peak at 2.5 eV is the second harmonic generation (SHG) emission. The two-photon origin of these emissions is further confirmed in Fig. 1b inset. Both the TPL and SHG signals show a quadratic power dependence, suggesting that the emission is indeed induced by two-photon absorption. The TPL saturates at higher power as a consequence of heating or exciton–exciton annihilation effects[21,22]. The trion peak amplitude is selected as our TPL signal.

We collect the TPL signal, while scanning the excitation laser energy from 2.05 to 2.6 eV, to acquire the full two-photon spectrum. We observed two important resonances of similar linewidths in the two-photon spectrum, occurring at 2.28 and 2.48 eV, corresponding to two excitonic dark excited states (Fig. 2). The absorption spectrum of a WS_2 monolayer is plotted for comparison, where the A exciton (the 1*s* state) and its trion result in two absorption peaks at 2.04 eV and 2 eV, respectively. Near these one-photon resonances, TPL is negligible, consistent with the 1*s* nature of these states. On the other hand, no significant one-photon absorption is observed near the excitonic dark states, except for the B exciton (the other 1*s* state) at 2.45 eV which results from the spin–orbit splitting in the valence band. Such a complementary feature reflects the symmetry of the observed excitonic states. Hence, we label the TPL peaks as the 2*p* and 3*p* state of the A exciton series. Accordingly, the 1*s*–2*p* and 1*s*–3*p* separations are 0.24 eV and 0.44 eV, respectively. The extraordinarily large 1*s*–*np* (n = 2, 3) separations suggest that the exciton binding energy, defined as the separation between the 1*s* exciton ground state and the conduction band edge, is larger than 0.44 eV, which also indicates a significant self-energy contribution to the quasi-particle bandgap. Our discovery demonstrates that the previously claimed band-to-band transition mechanism in the optical response of monolayer WS_2 is inaccurate, as we show here that the optical response is dominated by excitonic states within the bandgap, in agreement with the GW-BSE calculation of MoS_2 (ref. 14). The real quasiparticle bandgap is much larger than previously reported. This finding is expected be general for other TMDC monolayers of similar structure.

We used the *ab initio* GW method[18] to calculate the quasiparticle band structure and the *ab initio* GW-BSE approach[19] to calculate the excitonic states and optical spectrum of a WS_2 monolayer (Fig. 3a), employing the BerkeleyGW package[23]. The principal and orbital quantum numbers of

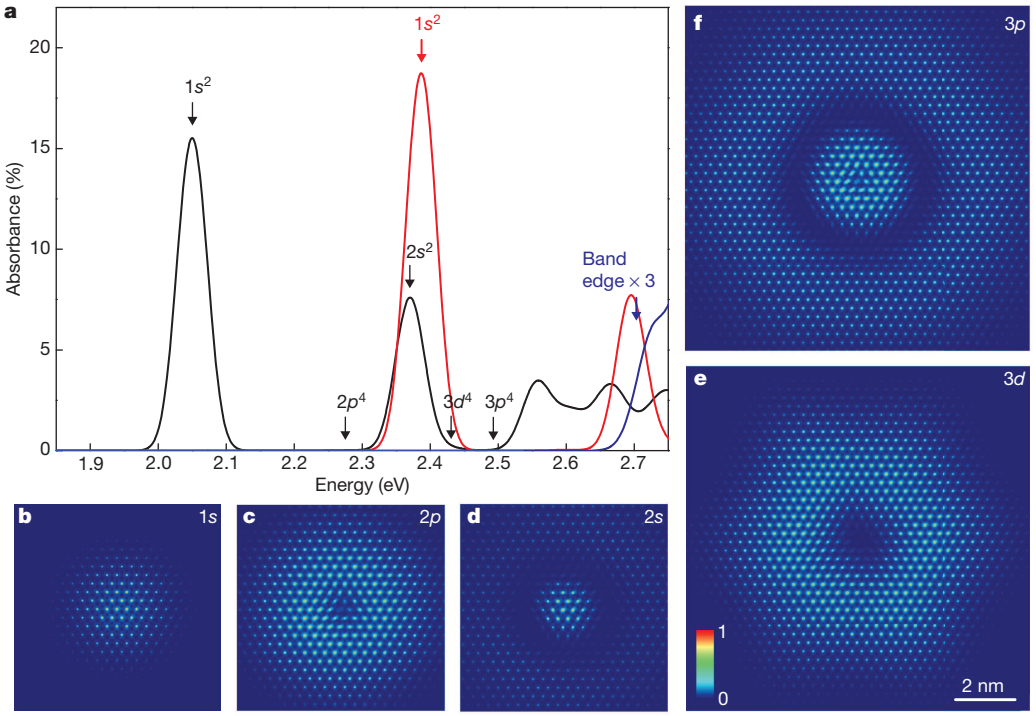

Figure 3 | One-photon absorption spectra and real-space exciton wavefunctions in monolayer WS_2 from *ab initio* GW-BSE calculations. **a**, The optical absorption of the A (black) and B (red) exciton series considering electron–hole interaction. The blue curve is the optical absorption spectrum, obtained without considering electron–hole interaction, where the quasiparticle bandgap is about 2.7 eV (blue arrow). The excitonic states of A and B exciton series, with electron–hole interaction included, are calculated (shown in **b**–**f**, see below) and labelled (in **a**) by black and red arrows, respectively, up to 2.5 eV. The computed 1*s*, 2*p* and 3*p* states of the A exciton are at 2.05 eV, 2.28 eV and 2.49 eV, respectively, and are in excellent agreement with the experimental measurements. Although the orbital notation of a 2D hydrogen atom is adopted to label the exciton states, the excitonic series significantly deviates from a hydrogenic series, as discussed in the main text. The degeneracy labels in the superscript include both the degeneracy of valleys and orbital angular momentum. **b**–**f**, The plots are modulus squared of the real-space exciton wavefunction projected onto the WS_2 plane, with the hole position fixed near a W atom at the centre of the plot. These wavefunctions share similar in-plane nodal structures with the excited states in a hydrogen atom, and therefore enable the eigenstates to be labelled with a principal and an orbital quantum number. The Wannier nature of the excitons is clear, with the radii much larger than the unit cell. The colour scale is the normalized wavefunction probability and applies to panels **b**–**f**.

each exciton state are identified by analysing the character of the exciton's real-space wavefunction (Fig. 3b–f). Specifically, the nodal characters along the radial direction are unique for each exciton state and have a one-to-one correspondence with those of the 2D Rydberg series. Consistent with the selection rule of one-photon absorption for dipole-allowed materials, we find that the '*s*' state is one-photon active or bright, while the other ('*p*' and '*d*') excitons are one-photon inactive or dark (see detailed analysis in Supplementary Information section S2). Clearly, the calculated 2*p* and 3*p* states, marked at 2.28 and 2.49 eV in Fig. 3a, agree well with the experimental results, which confirms our observation of dark excitonic states in WS_2 monolayer. The calculated positions of the 1*s* state of the A exciton series (2.04 eV) and B exciton series (2.4 eV) also agree well with the experimental spectrum. As is evident from the real-space wavefunctions in Fig. 3b–f, the excitons in monolayer WS_2 have a Wannier nature, with their in-plane radii much larger than the unit cell dimension. As mentioned above, owing to the broken inversion symmetry of the TMDC monolayer, the linear absorption selection rule is not exact. The exciton *p* states acquire a small but finite oscillator strength in our calculation, with the oscillator strength two orders of magnitude smaller than that of the *s* state in the same shell.

In spite of its Wannier character, we found that the exciton series in monolayer WS_2 deviates significantly from a 2D hydrogen model. Much smaller splitting between 1*s* and other excited states is observed, in accordance with recent GW-BSE calculations[14] (see detailed comparisons in Supplementary Information section S4). In addition, in a hydrogen atom, orbitals with the same principal quantum number are degenerate. However, for the WS_2 excitons, our calculations show that states in the same shell but of higher orbital angular momentums are at lower energy levels, that is, $E_{3d} < E_{3p} < E_{3s}$. These two exotic energy-level behaviours are caused by a strong spatial-dependent dielectric screening: in an atomically thin semiconductor, the screening effect at more than a certain distance is weaker when the separation between the electron and hole is bigger, which is known as the anti-screening effect in 1D carbon nanotubes[24] and as the dielectric confinement effect in 2D quantum wells[25]. Since the wavefunction of excitonic states with higher principal or higher orbital quantum number features a larger nodal structure near the hole (that is, a larger average electron–hole separation), weaker screening at larger separation leads to enhanced Coulomb attraction in the excited states and therefore a lowering of their excitation energies as compared with those of the hydrogen model[24]. Also, because of the degeneracy of the K and K′ valleys in the TMDC system, each *s* level has two degenerate states, while each *p* and *d* level has four degenerate states if perfect rotational symmetry is assumed. All of these features are expected to be quite general for 2D TMDC excitons.

The GW quasiparticle bandgap is calculated to be ~ 2.7 eV, indicated by the blue arrow in Fig. 3. Comparing this with the 1*s* exciton energy found in either our experiments or our GW-BSE calculations, we obtain an exciton binding energy of ~0.7 eV. Such an exceptionally large binding energy is more than ten times that found for the excitons in bulk WS_2 (ref. 3) and other traditional bulk semiconductors such as Si and GaAs (ref. 16), and comparable to those found for excitons in carbon nanotubes[20,26]. The large binding energy results from the combined effects of reduced dimensionality, relatively large effective masses and weak dielectric screening, which renders the excitons observable even at room temperature. Similar effects were also found in carbon nanotubes and inorganic-organic hybrid perovskites[20,27].

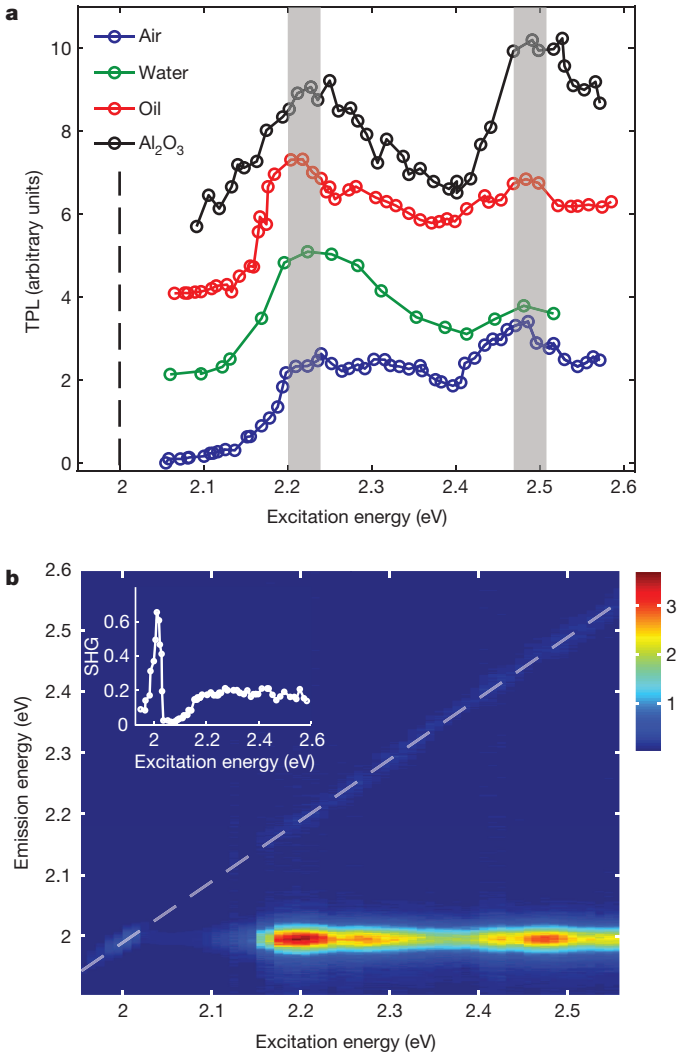

Figure 4 | Excitonic energy levels are robust to changes in the dielectric environment and to temperature changes. a, Room-temperature two-photon spectra of single-layer WS_2 with different top capping layers that tune the dielectric environment immediately adjacent to the atomic layer. The curves respectively represent the uncapped ($\varepsilon_{ave} = 1.625$, where ε_{ave} is the average dielectric constant between capping layers and the substrate), water capped ($\varepsilon_{ave} = 1.97$), immersion-oil capped ($\varepsilon_{ave} = 2.25$) and Al_2O_3 capped ($\varepsilon_{ave} = 2.57$) samples, and each curve is adjusted to a similar vertical scale and shifted for better visualization. The emission peak is at 2 eV, marked by the vertical black dashed line. Evidently, the 2*p* and 3*p* peak positions remain roughly unchanged within experimental error, marked by the grey bands at 2.22 ± 0.02 eV and 2.49 ± 0.02 eV, respectively. Therefore, the 1*s*–*np* ($n = 2, 3$) separation is approximately the same as the low-temperature uncapped result (Fig. 2), suggesting that the excitation energy of the low-energy exciton levels are relatively insensitive to dielectric environmental and temperature perturbations, as discussed in the main text. **b**, Main panel: measured emission spectra at different excitation energies of an immersion-oil capped WS_2 monolayer at room temperature. The horizontal line signal is the TPL emission, with two hotspots along the line corresponding to the 2*p* and 3*p* two-photon absorption peaks. Colour scale represents the normalized emission intensity. The SHG signal due to the broken inversion symmetry in the monolayer is observed (along the dashed line as an eye guide). At the intersection between the SHG and TPL line, the SHG signal experiences an excitonic enhancement from the A exciton 1*s* state (inset).

The excitonic ground state and low-energy excited states with large binding energy are robust to environmental perturbations owing to the opposite effects of the dielectric screening on the exciton binding energy and the quasiparticle self-energy[20,28]. We demonstrate this by measuring two-photon spectra of monolayer WS_2 with different dielectric capping layers, including water, immersion oil and aluminium oxide; the average dielectric constants of these capping layers at optical frequency range from 1.7 to 2.5. In all capped samples, we observed the 2*p* and 3*p* resonances even at room temperature (Fig. 4a). We find no significant shift in the excitation energy of either the *s* or the *p* states with different capping layers, except for an overall temperature-related redshift (0.04 eV) and linewidth broadening compared with measurements at 10 K (Fig. 2). The 1*s*–2*p* and 1*s*–3*p* energy differences remain roughly unchanged, ~0.2 and 0.5 eV, respectively. This robustness indicates that the measured excitation energies for the 2*p* and 3*p* states are intrinsic to the monolayer, thus agreeing well with those from an *ab initio* GW-BSE calculation for the vacuum condition. Together with the TPL signal, SHG is also observed as a slanted straight line in the excitation-emission spectra (Fig. 4b). At room temperature, the exciton–trion separation is no longer distinguishable, but the 2*p* and 3*p* absorption peaks remain prominent. An SHG resonance occurs as the TPL and SHG lines cross each other, and this resonance is known as the exciton enhanced SHG effect[29].

We have experimentally revealed 2D excitonic dark states in a WS_2 monolayer. These observations unveil an intense many-electron effect in this class of 2D gapped systems. The determined bandgap size would allow us to accurately design heterostructures consisting of a TMDC monolayer and other materials. Our discovery of extraordinarily strong excitons in a TMDC provides a basis for exploiting the unusual light–matter interactions resulting from strong many-electron effects, and should also help the development of emerging 2D electronic and optoelectronic applications.

Received 29 January; accepted 31 July 2014.
Published online 27 August 2014.

1. Wang, Q. H., Kalantar-Zadeh, K., Kis, A. & Coleman, J. N. Electronics and optoelectronics of two-dimensional transition metal dichalcogenides. *Nature Nanotechnol.* **7,** 699–712 (2012).
2. Radisavljevic, B., Radenovic, A., Brivio, J., Giacometti, V. & Kis, A. Single-layer MoS_2 transistors. *Nature Nanotechnol.* **6,** 147–150 (2011).
3. Beal, A. R., Knights, J. C. & Liang, W. Y. Transmission spectra of some transition metal dichalcogenides. II. Group VIA: trigonal prismatic coordination. *J. Phys. C* **5,** 3540–3551 (1972).
4. Mak, K. F., Lee, C., Hone, J., Shan, J. & Heinz, T. F. Atomically thin MoS_2: a new direct-gap semiconductor. *Phys. Rev. Lett.* **105,** 136805 (2010).
5. Splendiani, A. *et al.* Emerging photoluminescence in monolayer MoS_2. *Nano Lett.* **10,** 1271–1275 (2010).
6. Zeng, H., Dai, J., Yao, W., Xiao, D. & Cui, X. Valley polarization in MoS_2 monolayers by optical pumping. *Nature Nanotechnol.* **7,** 490–493 (2012).
7. Mak, K. F., He, K., Shan, J. & Heinz, T. F. Control of valley polarization in monolayer MoS_2 by optical helicity. *Nature Nanotechnol.* **7,** 494–498 (2012).
8. Cao, T. *et al.* Valley-selective circular dichroism of monolayer molybdenum disulphide. *Nature Commun.* **3,** 887 (2012).
9. Mak, K. F. *et al.* Tightly bound trions in monolayer MoS_2. *Nature Mater.* **12,** 207–211 (2012).
10. Ross, J. S. *et al.* Electrical control of neutral and charged excitons in a monolayer semiconductor. *Nature Commun.* **4,** 1474 (2013).
11. Britnell, L. *et al.* Strong light-matter interactions in heterostructures of atomically thin films. *Science* **340,** 1311–1314 (2013).
12. Ramasubramaniam, A. Large excitonic effects in monolayers of molybdenum and tungsten dichalcogenides. *Phys. Rev. B* **86,** 115409 (2012).
13. Cheiwchanchamnangij, T. & Lambrecht, W. R. L. Quasiparticle band structure calculation of monolayer, bilayer, and bulk MoS_2. *Phys. Rev. B* **85,** 205302 (2012).
14. Qiu, D. Y., Felipe, H. & Louie, S. G. Optical spectrum of MoS_2: many-body effects and diversity of exciton states. *Phys. Rev. Lett.* **111,** 216805 (2013).
15. Geim, A. K. & Grigorieva, I. V. Van der Waals heterostructures. *Nature* **499,** 419–425 (2013).
16. Knox, R. S. *Theory of Excitons* (Academic, 1963).
17. Scholes, G. D. & Rumbles, G. Excitons in nanoscale systems. *Nature Mater.* **5,** 683–696 (2006).
18. Hybertsen, M. S. & Louie, S. G. Electron correlation in semiconductors and insulators: band gaps and quasiparticle energies. *Phys. Rev. B* **34,** 5390–5413 (1986).
19. Rohlfing, M. & Louie, S. G. Electron-hole excitations and optical spectra from first principles. *Phys. Rev. B* **62,** 4927–4944 (2000).
20. Wang, F., Dukovic, G., Brus, L. E. & Heinz, T. F. The optical resonances in carbon nanotubes arise from excitons. *Science* **308,** 838–841 (2005).
21. Ye, Y. *et al.* Exciton-dominant electroluminescence from a diode of monolayer MoS_2. *Appl. Phys. Lett.* **104,** 193508 (2014).
22. Kumar, N. *et al.* Exciton-exciton annihilation in $MoSe_2$ monolayers. *Phys. Rev. B* **89,** 125427 (2014).
23. Deslippe, J. *et al.* BerkeleyGW: A massively parallel computer package for the calculation of the quasiparticle and optical properties of materials and nanostructures. *Comput. Phys. Commun.* **183,** 1269–1289 (2012).

24. Deslippe, J. *et al.* Electron-hole interaction in carbon nanotubes: novel screening and exciton excitation spectra. *Nano Lett.* **9,** 1330–1334 (2009).
25. Keldysh, L. V. Coulomb interaction in thin semiconductor and semimetal films. *J. Exp. Theor. Phys. Lett.* **29,** 658–660 (1979).
26. Spataru, C. D., Ismail-Beigi, S., Benedict, L. X. & Louie, S. G. Excitonic effects and optical spectra of single-walled carbon nanotubes. *Phys. Rev. Lett.* **92,** 077402 (2004).
27. Ishihara, T., Takahashi, J. & Goto, T. Optical properties due to electronic transitions in two-dimensional semiconductors $(C_nH_{2n+1}NH_3)_2PbI_4$. *Phys. Rev. B* **42,** 11099–11107 (1990).
28. Maultzsch, J. *et al.* Exciton binding energies in carbon nanotubes from two-photon photoluminescence. *Phys. Rev. B* **72,** 241402 (2005).
29. Malard, L. M., Alencar, T. V., Barboza, A. P. M., Mak, K. F. & de Paula, A. M. Observation of intense second harmonic generation from MoS_2 atomic crystals. *Phys. Rev. B* **87,** 201401 (2013).

Supplementary Information is available in the online version of the paper.

Acknowledgements This research was supported by the Lawrence Berkeley National Laboratory through the Office of Basic Energy Sciences, US Department of Energy under contract no. DE-AC02-05CH11231: the experimental work was supported by Sub-wavelength Metamaterial Design, Physics and Applications Program, and the theory part was supported by the Theory Program (GW-BSE calculations and simulations) and by the SciDAC Program on Excited State Phenomena (computer codes and algorithm developments), with computer time provided by the DOE National Energy Research Scientific Computing Center (NERSC). Z.Y. acknowledges discussions with T. Ishihara and F. Wang.

Author Contributions Z.Y. and X.Z. initiated this research topic; Z.Y., K.O., X.Y. and Y.W. conducted the optical experiments; Z.Y. and H.Z. prepared samples; T.C. and S.G.L. performed the first-principles calculations; Z.Y., T.C., S.G.L. and X.Z. analysed the results and prepared the manuscript. All authors contributed to discussions and manuscript revision.

Author Information Reprints and permissions information is available at www.nature.com/reprints. The authors declare no competing financial interests. Readers are welcome to comment on the online version of the paper. Correspondence and requests for materials should be addressed to X.Z. (xzhang@me.berkeley.edu) and S.G.L. (sglouie@berkeley.edu).